RESEARCH ARTICLE

Thermosensitive hydrogel-delivered Tanshinone IIA nanoparticles for enhanced periodontal tissue regeneration

Wenting Zou[1], Jing Hu[2,*], Yuxuan Gao[1], Bingjie Fan[1], Yaru Wang[1], Zhengguang Liu[3]

[1]Stomatology College, Jiamusi University, Jiamusi, Heilongjiang, China. [2]The Affiliated Stomatological Hospital, Jiamusi University, Jiamusi, Heilongjiang, China. [3]Department of Stomatology, Shuangyashan Stomatological Hospital, Shuangyashan, Heilongjiang, China.

Received: July 3, 2025; **accepted:** October 22, 2025.

Tanshinone IIA (TA) is a natural compound derived from *Salvia miltiorrhiza* with recognized anti-inflammatory and bone metabolism-promoting properties. However, its poor water solubility limits its clinical application, particularly in periodontal therapy where sustained local drug delivery is essential. To overcome this limitation, this study employed nanotechnology to encapsulate TA into nanoparticles (TA-NPs), which were further incorporated into a temperature-sensitive hydrogel system to enhance the bioavailability of TA and promote periodontal tissue regeneration using this novel delivery system. The hydrogel was prepared using chitosan, dextran, and β-glycerophosphate sodium *via* a self-assembly method. Its structure and properties were characterized by Fourier-transform infrared spectroscopy, scanning electron microscopy, transmission electron microscopy, and rheological analysis. *In vitro* experimental results using rat periodontal ligament stem cells (PDLSCs) demonstrated that the TA-NPs-loaded hydrogel exhibited no cytotoxicity and significantly promoted cell proliferation. *In vivo* studies in a rat periodontitis model revealed that the hydrogel possessed remarkable anti-inflammatory and alveolar bone regeneration effects. Micro-computed tomography (Micro-CT) analysis showed that the drug-loaded hydrogel group (Group E) had significantly higher bone volume fraction and bone mineral density compared to the model group ($P < 0.001$). Histological staining confirmed reduced inflammatory cell infiltration, clearer periodontal ligament structure, and lower collagen volume fraction in Group E ($P < 0.01$). The TA-NPs-loaded temperature-sensitive hydrogel developed offered a promising strategy for applying traditional Chinese medicine in periodontal treatment and presented a potential innovative material for periodontal tissue regeneration.

Keywords: Tanshinone IIA; temperature-sensitive hydrogel; nanoparticles; periodontal regeneration; stem cells.

[*]**Corresponding author:** Jing Hu, The Affiliated Stomatological Hospital, Jiamusi University, Jiamusi, Heilongjiang 154000, China. Email: hujing9481@163.com.

Introduction

Damage to periodontal tissues including the gums, ligament between the teeth, and alveolar bone is the hallmark of periodontal disease, an inflammatory disorder with a localized impact. Aside from the effects on oral health, the disease is also associated with systemic conditions [1]. Periodontitis, a severe manifestation of periodontal disease, has a complex pathogenesis involving microbial dysbiosis, aberrant host immune responses, lifestyle factors, and systemic diseases. The World Health Organization (WHO) has recognized periodontitis

as a major contributor to tooth loss [2], affecting approximately 743 million people globally with a prevalence of 11.2% [3]. Periodontitis is often considered a "silent" disease as it rarely presents with overt symptoms and signs in its early stages, typically becoming apparent only when the disease has developed to an advanced stage. If left untreated, periodontitis may ultimately lead to the destruction of tooth-supporting structures with severe periodontitis potentially resulting in tooth loss, thereby significantly reducing the quality of life [4]. Nevertheless, periodontitis is not merely a localized condition. Periodontal pathogens, their metabolic products, and inflammatory mediators can enter the systemic circulation, thereby triggering the development of systemic diseases [5]. A growing body of research data suggests that periodontitis has clear associations with multiple systemic conditions [6]. The relationship between periodontitis and diabetes, metabolic syndrome, cardiovascular disease, and chronic kidney disease has been well-established [7-9]. The link between periodontitis and several other conditions like Alzheimer's disease, adverse pregnancy outcomes, and cancer is under further investigation and awaits confirmation [10-12]. In periodontal therapy, conventional subgingival scaling and root planning demonstrate limited efficacy. Hence, adjunctive pharmacological interventions, particularly broad-spectrum antibiotics, have emerged as therapeutic options for controlling periodontal infections. However, antimicrobial resistance amongst periodontal pathogens presents an increasingly significant challenge [13].

Antibiotic resistance in periodontal disease patients has been on the rise in recent years [14]. The unique periodontal environment and biofilm formation further reduce bacterial susceptibility to antibiotics, thereby complicating treatment outcomes [15]. Traditional Chinese medicine (TCM) has garnered increasing attention in periodontitis treatment, primarily due to its safety profile and therapeutic efficacy [16]. *Salvia miltiorrhiza* with its millennial research history ranks amongst China's most frequently utilized traditional herbs [17]. Tanshinone, a lipid-soluble diterpenoid quinone compound isolated from dried *Salvia miltiorrhiza* roots, represents its primary pharmacological constituent [18]. Tanshinone IIA (TA) is another crucial component, exhibiting diverse pharmacological properties including anti-tumor, antioxidant, antimicrobial [19], anti-inflammatory, and osteogenic effects [20]. Nevertheless, its clinical application remains limited due to poor solubility, permeability, and bioavailability [21]. Nanotechnology has emerged as an effective approach to enhance existing drug efficacy [22]. Nanoparticle drug delivery systems can protect drugs from premature degradation [23], enhance cellular penetration, and improve drug absorption [24]. Natural proteins, serving as carriers for hydrophobic bioactive components, offer advantages including degradability and low immunogenicity, enabling stable encapsulation of TA and improving overall nanoparticle solution stability [25]. Hydrogels, as typical biological scaffolds, feature highly hydrated three-dimensional network structures, favorable biodegradability, and adjustable mechanical properties [26], which provide suitable microenvironments for cells and find widespread applications in tissue engineering and cellular therapy [27]. Given that oral topical drug delivery is susceptible to dilution by saliva, oral therapeutic gels should possess drug loading, adhesion, and sustained-release properties [28]. Chitosan, a naturally occurring polymer with biodegradability, inherent antimicrobial properties, and excellent biocompatibility, is extensively employed in tissue engineering and drug delivery [29, 30].

This study investigated the preparation of thermosensitive hydrogels loaded with Tanshinone IIA nanoparticles (TA-NPs) and their impact on periodontal tissue regeneration. Through both *in vitro* and *in vivo* experiments, the cytotoxicity and therapeutic efficacy in periodontal bone defects were examined, potentially offering novel strategies for periodontitis treatment.

Materials and methods

Preparation of TA-NPs

300 mg sodium caseinate (Sigma-Aldrich, St. Louis, MO, USA) was dissolved in 150 mL of 10 mM PBS buffer (pH 8.3), while 5 mg trypsin (1:60 enzyme-to-substrate ratio) (w/w) was added to the solution and incubated at 50°C for 6 h with continuous stirring at 250 rpm. The enzymatic reaction was terminated by boiling for 10 min followed by centrifugation at 6,500 ×g for 10 min at 4°C to remove insoluble residues. The supernatant was lyophilized and stored at -20°C until use. 300 mg Lyophilized NaCas/Eh was reconstituted in 10 mL deionized water. 10 mg Tanshinone IIA (Chengdu Herbpurify Co., Ltd., Chengdu, Sichuan, China) was dissolved in 4 mL ethanol and gradually added to the NaCas/Eh solution under vortex mixing at 2,000 rpm. The mixture underwent self-assembly at 37°C for 24 h followed by ethanol removal through rotary evaporation at 43°C. Unencapsulated TA was eliminated by centrifugation at 7,000 ×g for 5 min, and the nanoparticle-containing supernatant was stored at 4°C. TA-NPs were disrupted with ethanol (1:4, v/v) and filtered through 0.22 µm PVDF membrane (Millipore, Billerica, MA, USA). TA content was quantified by using Agilent 1260 Infinity II HPLC system (Agilent Technologies, Santa Clara, CA, USA) with C18 column, methanol/water (75:25) mobile phase, 1 mL/min flow rate, and 270 nm detection. Encapsulation efficiency (EE) was then calculated as below.

EE (%) = (Encapsulated TA amount/Total TA input) × 100%

Hydrogel preparation

Chitosan-based hydrogels were prepared through a cold-induced gelation method. Chitosan/β-glycerophosphate (CS/β-GP) hydrogel was prepared by dissolving 2.0% Chitosan (degree of deacetylation ≥ 95%) (Shanghai Yuanye Bio-Technology Co., Ltd., Shanghai, China) in 0.1 M acetic acid under magnetic stirring at 500 rpm for 24 h. 60% β-GP solution was added dropwise to the chitosan solution at a 3:7 volume ratio (β-GP:CS) under vortex mixing. The mixture was sonicated at 40 kHz for 10 s and incubated at 37°C for 5 min to induce gelation. CS/DEX/β-GP hydrogel was prepared by incorporating 1.5% Dextran into the chitosan solution prior to β-GP addition, maintaining identical gelation conditions. CS/DEX/β-GP/TA-NPs hydrogel was prepared by using 60% TA-NPs/β-GP suspension (containing 0.6 mg/mL TA) to replace pure β-GP solution during the mixing step. All hydrogels were stored at 4°C until characterization.

Appearance characterization

Photographic documentation of the three chitosan-based hydrogel mixtures (CS/β-GP, CS/DEX/β-GP, CS/DEX/β-GP/TA-NPs) before and after gelation was conducted to visually assess hydrogel formation. 3 to 5 mg of sample was mixed with approximate 5% dried potassium bromide powder in a mortar. The mixture was pressed into a thin film under vacuum pressure of 20 mmHg for 5 min. A Nicolet iS50 spectrometer (Thermo Fisher Scientific, Waltham, MA, USA) was employed for Fourier-Transform Infrared (FTIR) spectroscopy with a scanning range of 4,000 – 500/cm. A Hitachi SU8010 field emission scanning electron microscope (Hitachi, Tokyo, Japan) was used for surface morphology observation. Briefly, 400 µL of prepared hydrogel was pre-frozen at -20°C and then freeze-dried. The sample surface was gold-sputtered for 30 seconds to enhance conductivity. The morphology of Tanshinone IIA nanoparticles (TA-NPs) was also observed using a Hitachi HT-7800 transmission electron microscope (Hitachi High-Technologies Corporation, Tokyo, Japan) at an acceleration voltage of 100 kV by applying a droplet of the TA-NPs suspension onto a carbon-coated copper grid and air-dry at room temperature.

Rheological performance analysis

CS/β-GP, CS/DEX/β-GP, and CS/DEX/β-GP/TA-NPs hydrogel solutions were placed on a DHR-2 rotational rheometer (TA Instruments, New Castle, DE, USA) at a frequency of 1 Hz and a strain amplitude of 0.01%. Storage modulus (G') and loss modulus (G") were noted across a temperature range of 10 - 50°C.

Swelling ratio determination

Initial weight (W_0) of each hydrogel was measured. Samples were immersed in PBS buffer (pH 7.4) at 37°C and weighed at different time points after surface water removal (W_t). Swelling ratio was calculated as follows.

$$\frac{W_t - W_0}{W_0} \times 100\%$$

***In vitro* degradation performance test**

On a constant-temperature shaker set at 37°C and 70 rpm, precisely weighed freeze-dried hydrogels were submerged in a PBS solution containing 1,000 U/mL of lysozyme. After being rinsed with ultrapure water, the samples were freeze-dried and weighed (W_t) at predetermined intervals. Hydrogel weight retention rate was calculated accordingly as below.

$$\frac{W_t}{W_0} \times 100\%$$

Tanshinone standard curve and *in vitro* drug release experiment

2 mg of TA powder was precisely weighed and dissolved in 2 mL of methanol solution to prepare the stock solution. Through serial dilution, TA standard solutions were prepared at the concentrations of 20, 10, 5, and 2.5 μg/mL. 1 mL of each standard solution was transferred to a quartz cuvette to determine the absorbance at 268 nm using an ultraviolet spectrophotometer. Linear regression analysis between absorbance values and corresponding concentrations was performed to obtain the standard curve and calculate the linear regression equation with a requirement of $R^2 > 0.99$. CS/DEX/β-GP/TA-NPs hydrogel samples were placed in 3 mL of PBS solution and incubated at 37°C and 70 rpm. PBS supernatants were collected at various intervals and substituted with the same volume of fresh PBS. The TA concentration in the supernatant was determined using the pre-established standard curve by using ultraviolet spectrophotometry. The cumulative release rate (%) was calculated by dividing cumulative drug release amount with the total drug content.

Blood compatibility experiment

The blood samples were collected from healthy SD rats' hearts. After multiple washing and centrifugation at 2,000 rpm for 5 min, the precipitated red blood cells were collected and mixed with PBS at a 1:16 ratio to prepare a red blood cell-rich solution (RBC). 1 mL of hydrogel samples were immersed in a mixed solution of 1 mL RBC and 4 mL PBS and incubated at 37°C for 2 h before centrifugation at 3,500 rpm for 5 min followed by measuring the absorbance of the supernatant at 540 nm using a Multiskan SkyHigh microplate reader (Thermo Fisher Scientific, Waltham, MA, USA). The positive control group consisted of a mixture of 1 mL RBC and 4 mL deionized water, while the negative control group comprised 1 mL RBC and 4 mL PBS. The hemolysis rate (H) was calculated using the following formula.

$$\mathrm{H} = \frac{D_t - \mathrm{D}_{nc}}{\mathrm{D}_{pc} - \mathrm{D}_{nc}} \times 100\%$$

where D_t was the absorbance value of the test sample. D_{nc} was the negative control group. D_{pc} was the positive control group. H was the hemolysis rate (%).

***In vitro* evaluation of hydrogel based therapeutic platform for periodontitis**

(1) Cell culture

Rat periodontal ligament stem cells (PDLSCs) were purchased from Wuhan Punosei, Wuhan, Hubei, China and cultured at a density of 5×10^5 cells/T25 flask in DMEM high-glucose medium supplemented with 10% fetal bovine serum (FBS) under 37°C. At 70 - 90% cell confluence, the initial medium was removed followed by washing cells twice with sterile PBS and then treating with 1 mL of 0.25% trypsin for 1 min. Once the cells appeared round under the microscope, the same volume of serum-containing medium was integrated to terminate the digestion. The cells were then dislodged by pipetting and collected into a 15 mL centrifuge tube before centrifugation at 1,000 rpm for 5 min. The cells were resuspended in fresh medium and adjusted to a density of 2×10^4/mL.

(2) Cell proliferation cytotoxicity assay

The adjusted PDLSCs were seeded into a 96-well plate with 100 µL of medium added to each well. A blank control group and various hydrogel intervention groups were set up at the concentrations of 5, 10, 15, 20, and 25 µM. The cells grew at 37°C with 5% CO_2. The CCK-8 assay (Beijing Solarbio, Beijing, China) was performed at 24, 48, and 72 h after incubation by adding 10 µL of CCK-8 solution to each well and incubating for 2 h. The absorbance at 450 nm was obtained by using Multiskan 51119 microplate reader (Thermo Fisher, Waltham, MA, USA). The relative proliferation rate (RPR) of the cells was calculated to evaluate cell proliferation as follows.

$$RPR=(OD_{control}-OD_{blank})/(OD_{experiment}-OD_{blank})\times 100\%$$

(3) Drug concentration verification

To verify the toxicity and optimal concentration of tanshinone IIA-loaded nanoparticles (TA-NPs) on PDLSCs, the cell density was changed to 2×10^4/mL and seeded into a 96-well plate with 100 µL of medium in each well. A blank control group and different concentrations of TA-NPs intervention groups of 5, 10, 15, 20, and 25 µM were set up and cultured at 37°C with 5% CO_2. The CCK-8 assay was performed at 24 h, 48 h, and 72 h after culture. RPR was calculated to evaluate the influences of different concentrations of TA-NPs on cell proliferation. The optimal drug concentration without cytotoxicity was determined.

***In vivo* therapeutic efficacy assessment of hydrogel in periodontitis animal model**

(1) Animal model construction and treatments

A total of 15 8-week-old male Sprague-Dawley (SD) rats purchased from Shanghai Bikai Keyuan Biological Technology Co., Ltd. (Shanghai, China) were used in this research. After one week of adaptive feeding, the rats were anaesthetized using 30 mg/kg sodium pentobarbital. The left maxillary first molar was exposed. The gingiva was separated using a dental probe, and a 0.25 mm diameter orthodontic ligature wire was tied around the cervical region of the maxillary first molars bilaterally to induce periodontitis. The rats of blank control group received no treatment. After 4 weeks, all animals underwent oral clinical examination. The treated model group showed gingival swelling, tooth loosening, and periodontal pocket formation, indicating successful model establishment. After successfully establishment of the periodontitis model at 4 weeks, the rats were randomly divided into five groups with 3 animals in each group, which included blank control (group A) without any ligature or treatment, model control (group B) with periodontitis that received no subsequent treatment, free drug group (group C) with periodontitis that received a local injection of tanshinone IIA solution at a dose equivalent to that in the hydrogel into the periodontal pocket, blank hydrogel group (group D) with periodontitis that received the plain thermosensitive hydrogel CS/DEX/β-GP without TA-NPs injected into the periodontal pocket, drug-loaded hydrogel group (group E) with periodontitis that received the TA-NPs-loaded thermosensitive hydrogel CS/DEX/β-GP/TA-NPs injected into the periodontal pocket. All animal experimental procedures were approved by the Animal Ethics Committee of Jiamusi University, Jiamusi, Heilongjiang, China.

(2) Micro-CT analysis

Micro-CT scanning was applied to assess the changes in bone tissue of the maxilla in each group. The left maxillary bone tissue was fixed and then scanned using a SkyScan 1276 micro-CT scanner (Bruker, Kontich, Belgium) with 200 µA current, 85 kV voltage, 9.054195 µm scan resolution, 240 ms exposure time, and 180° scan angle. The original images were reconstructed using the NRecon (V1.7.4.2) software (Bruker, Kontich, Belgium) with the smoothing, beam-hardening, and ring artifacts being set at 5, 8, and 25%, respectively. The region of interest (ROI) was analyzed using the CT Analyzer software (1.20.3.0) to calculate the total volume (TV), bone volume (BV), bone volume fraction (BV/TV), bone surface (BS), trabecular number (Tb.N), and trabecular thickness (Tb.Th).

(3) HE staining

HE staining was employed to monitor the pathological changes in the maxillary bone tissue of the rats. The fixed tissue was decalcified using EDTA decalcification solution for 30 days, dehydrated by graded ethanol, embedded in paraffin, sectioned at 5 μm thickness, and stained. The staining steps included xylene dewaxing, graded ethanol dehydration, haematoxylin staining for 5 - 10 min, acid-alcohol differentiation for 5 - 10 s, bluing at 37°C water bath for 10 min, and eosin staining for 2 - 3 min. The sections were mounted with neutral balsam, observed under an optical microscope, and photographed the pathological changes.

(4) Masson's trichrome staining

Masson's trichrome staining was used to evaluate the distribution and content of collagen fibers. The staining steps included xylene dewaxing, graded ethanol dehydration, Weigert's haematoxylin staining for 5 - 10 min, acid-alcohol differentiation for 5 - 15 s, Masson's blue staining for 3 - 5 min, Ponceau-fuchsin staining for 5 - 10 min, weak acid treatment for 1 min, phosphomolybdic acid solution washing for 1 - 2 min, and aniline blue staining for 1 - 2 min. The sections were mounted with neutral balsam. The collagen volume fraction (CVF) was analyzed using the Image-Pro Plus 6.0 software (Media Cybernetics, Rockville, MD, USA) to evaluate the collagen fiber content.

(5) Enzyme-linked immunoassay (ELISA)

ELISA was used to evaluate the levels of the inflammatory factors IL-1β and IL-18 in the rat serum. Frozen rat serum samples were taken out of the -20°C freezer 12 h in advance and thawed at 4°C for 12 h. Rat IL-1β and IL-18 ELISA kits (Shanghai Keaibao Biology, Shanghai, China) were used following the manufacturer's instructions. The OD values were measured at 450 nm using a Multiskan SkyHigh microplate reader, and the sample concentrations were calculated based on the standard curve.

Statistical analysis

The quantitative data was presented as mean ± standard error (Mean ± SEM). GraphPad Prism 8.0 software (https://www.graphpad.com) was used for statistical analysis and data visualization. Unpaired t-test was used to compare the difference between two groups, while one-way ANOVA was used to compare the difference among multiple groups. $P < 0.05$ was considered as statistically significant difference.

Results

Material characterization

(1) Appearance and structural characterization of hydrogel

The formation process of the hydrogel showed that, under constant temperature of 37°C, the amino groups ($-NH_3^+$) on the chitosan chain generated electrostatic repulsion in an acidic environment due to positive charges (Figure 1A). Upon introducing negatively charged β-glycerophosphate ($-PO_4^{3-}$), electrostatic repulsion was significantly reduced. Simultaneously, the glycerol portion of β-GP interacted with water, promoting chitosan chain hydration and allowing free chain extension in solution (Figure 1B). As temperature increased, hydrogen bonds between chitosan and water were disrupted, water molecules were released, and chitosan chains became more closely arranged, ultimately forming a gel through hydrophobic interactions between polymer chains (Figure 1C).

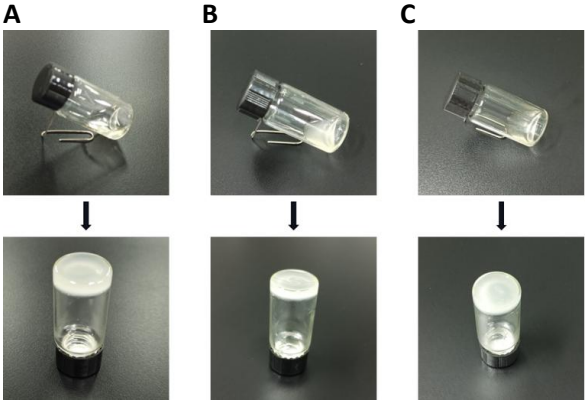

Figure 1. Formation process of hydrogel.

(2) FTIR analysis

FTIR analysis revealed that chitosan (CS) exhibited O-H and N-H stretching vibration peaks at 3,430/cm and a C = O vibration peak at 1,606/cm. β-GP showed an O-H stretching vibration peak at 3,411/cm with asymmetric and symmetric $-PO_4^{3-}$ stretching vibration peaks at 1,125/cm and 979/cm, respectively. In the CS/DEX/β-GP hydrogel, the $-PO_4^{3-}$ stretching vibration peak red-shifted from 1,125/cm to 1,118/cm, indicating β-GP's participation in the hydrogel's crosslinking network. Furthermore, the peak's subsequent red-shifted to 1,120/cm with reduced intensity suggested new hydrogen bond formation between DEX and β-GP (Figure 2).

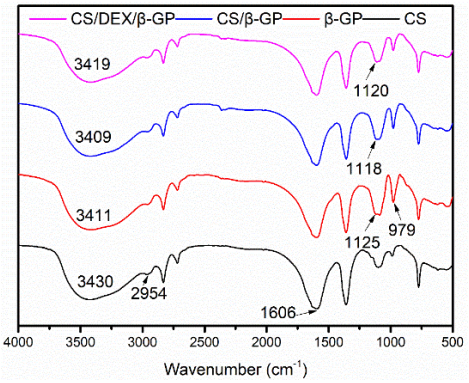

Figure 2. FTIR spectra of CS, β-GP, CS/β-GP, and CS/Dex/β-GP.

(3) SEM and TEM analysis

SEM observations revealed three-dimensional porous structures for CS/β-GP, (CS/Dex)/β-GP, and (CS/Dex)/(TA-NPs/β-GP) hydrogels with pore sizes ranging between 100 - 250 µm. TEM examination of TA-NPs showed dense, uniformly distributed spherical structures.

(4) Rheological analysis

Rheological tests demonstrated a phase transition temperature of 34.5°C for CS/β-GP, CS/DEX/β-GP, and CS/DEX/β-GP/TA-NPs hydrogels. When temperature was below 34.5°C, the hydrogels exhibited a liquid flow state with G' < G'', while the temperature was above 34.5°C, G' was significantly larger than G'', indicating gel formation. Additionally, DEX incorporation substantially increased G', suggesting enhanced mechanical properties (Figure 3).

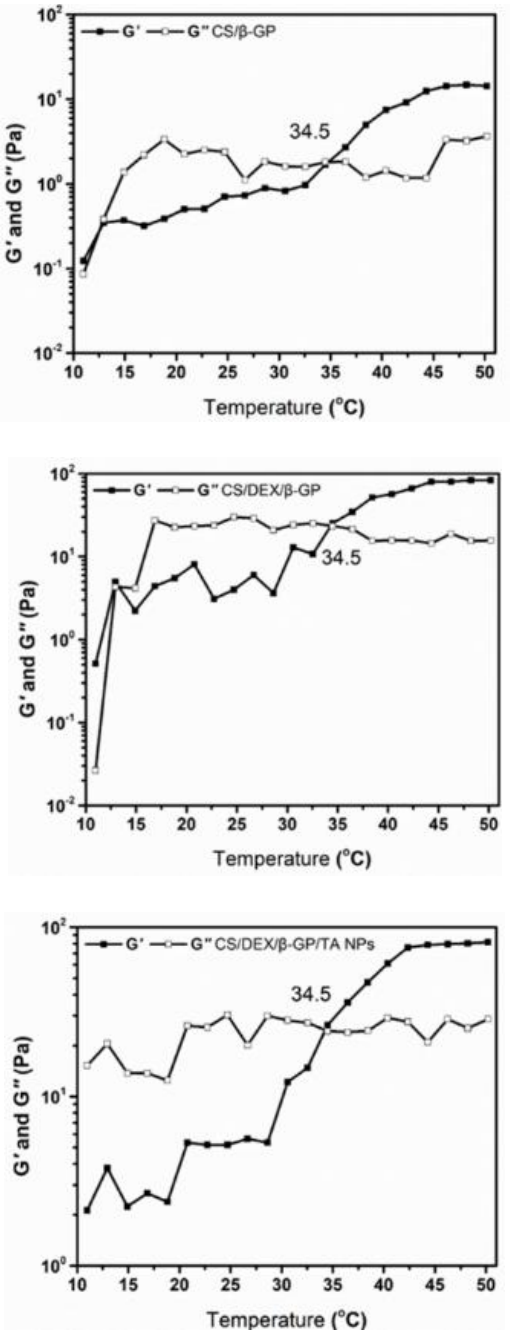

Figure 3. Changes in G' and G" of CS/β-GP, CS/DEX/β-GP, and CS/DEX/β-GP/TA-NPs hydrogels with temperature. The temperature at which G' = G" was the gelation temperature.

(5) *In vitro* drug release curve

A standard curve for TA was established to quantify the drug release kinetics, which

demonstrated excellent linearity (R^2 > 0.99) within the tested concentration range (Figure 4). The TA-NPs exhibited a tannic acid encapsulation rate of 92.4 ± 2.5%. The results showed that TA release was slower in CS/DEX/β-GP/TA-NPs compared to CS/β-GP/TA-NPs, indicating improved water stability. Both hydrogel formulations demonstrated linear release trends within the first 7 days with cumulative release rates of approximately 58.0% and 72.9%, respectively, followed by gradual release (Figure 5a). The controlled release mechanism likely involved nanoparticle degradation and concentration diffusion.

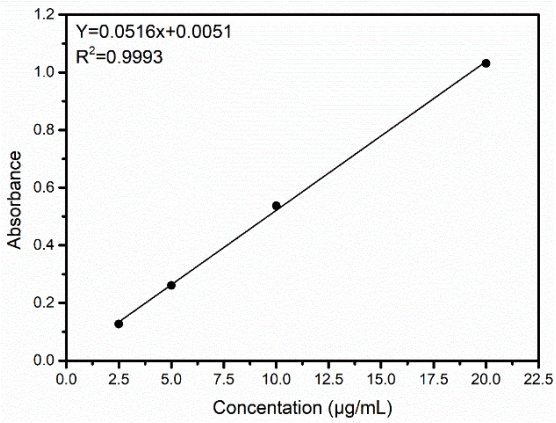

Figure 4. Standard curve of tanshinone.

(6) *In vitro* degradation curve

Polymer material degradation was crucial for biological applications. Initial rapid degradation resulted from insufficient β-GP crosslinking with subsequent reduced degradation rates. Over a 3-week period, the total degradation rate reached 80%. Degradation potentially occurred through enzymatic breakdown of chitosan and DEX chains. CS/DEX/β-GP/TA-NPs exhibited lower weight loss compared to CS/β-GP/TA-NPs, possibly due to hydrogen bond formation with DEX (Figure 5b).

(7) Hemolysis analysis

Hemolysis testing evaluated material biocompatibility by assessing red blood cell destruction. Lower hemolysis rates indicated better blood compatibility. The hydrogels demonstrated hemolysis rates below 5%, which was significantly below industry standards. The hemolysis test results demonstrated outstanding blood compatibility of the developed hydrogels. After 1, 4, and 8 hours of incubation, the hemolysis rates for both the plain hydrogel (CS/DEX/β-GP) and the drug-loaded hydrogel (CS/DEX/β-GP/TA-NPs) remained remarkably low, ranging from approximately 1.8% to 2.5% with CS/DEX/β-GP/TA-NPs group showing marginally lower hemolysis rates of 1.8%, 2.0%, and 2.2% at 1, 4, and 8 hours, respectively, compared to the plain hydrogel group of 2.1%, 2.3%, and 2.5%, respectively. Importantly, all measured values were significantly below the 5% safety threshold, indicating excellent hemocompatibility. In stark contrast, the positive control group consistently exhibited complete hemolysis of around 100%, validating the test conditions. These results confirmed that the hydrogel matrix itself was highly blood-compatible and that the incorporation of Tanshinone IIA nanoparticles did not induce any hemolytic risk.

***In vitro* performance of the hydrogel for periodontal disease treatment**

(1) Cell proliferation cytotoxicity

The cell proliferation cytotoxicity assay demonstrated that the hydrogel loaded with TA-NPs (CS/Dex/β-GP/TA-NPs) had no significant impact on the proliferation of rat PDLSCs. There was no discernible variation in the relative proliferation rate among the experimental groups compared with the control group (P > 0.05), indicating that the hydrogel composite exhibited no apparent cytotoxicity towards PDLSCs and had good biocompatibility *in vitro* (Figure 6).

(2) Drug concentration verification

The results showed that the concentration of 2 mg/mL TA-NPs had the least impact on cell proliferation, and the relative proliferation rate was not significantly different from the control group (P > 0.05) (Figure 7).

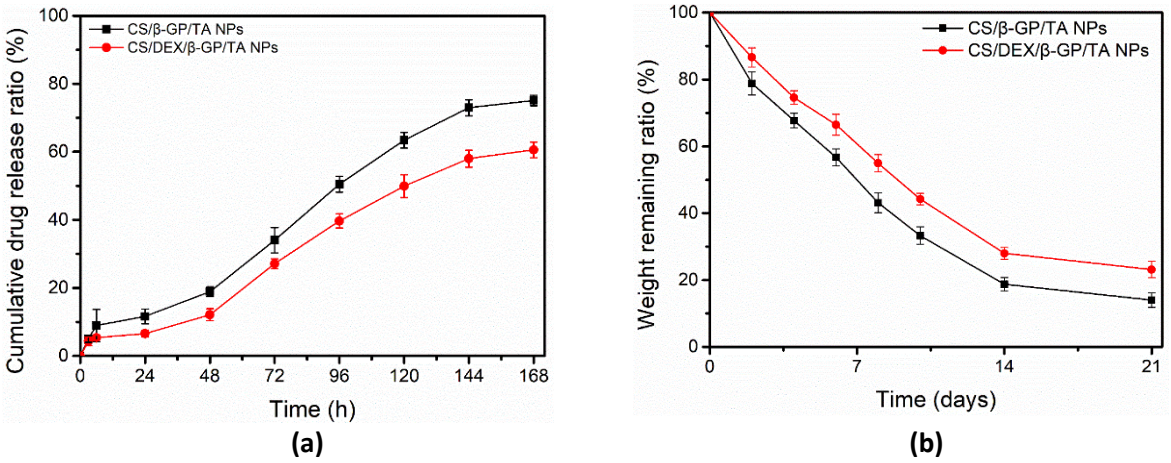

Figure 5. *In vitro* drug release profiles (a) and degradation curves (b) of CS/DEX/β-GP/TA-NPs and CS/DEX/β-GP/TA-NPs hydrogels.

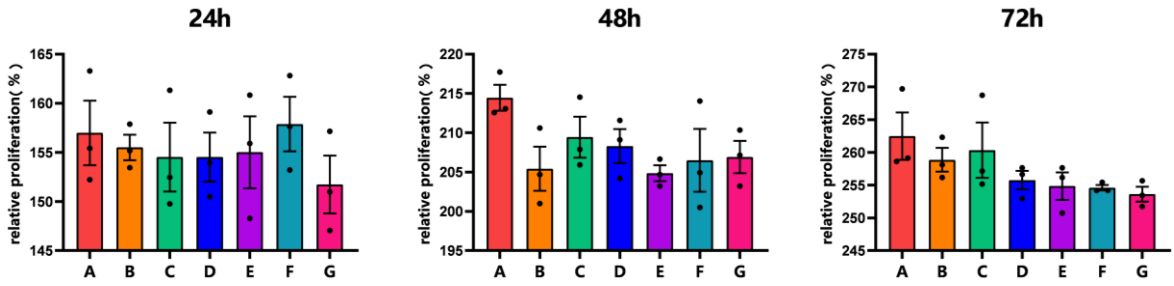

Figure 6. Biocompatibility of the hydrogel composites with rat PDLSCs (n = 3). **A.** Control group. **B.** Plain hydrogel group. **C.** Hydrogel + 5 μM tanshinone. **D.** Hydrogel + 10 μM tanshinone. **E.** Hydrogel + 15 μM tanshinone. **F.** Hydrogel + 20 μM tanshinone. **G.** Hydrogel + 25 μM tanshinone.

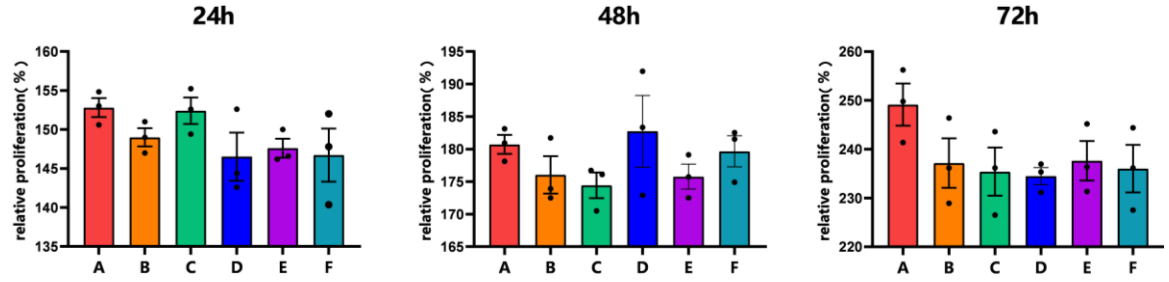

Figure 7. Drug concentration verification for rat PDLSCs (n = 3). **A.** Control group. **B.** 5 μM tanshinone. **C.** 10 μM tanshinone. **D.** 15 μM tanshinone. **E.** 20 μM tanshinone. **F.** 25 μM tanshinone.

In vivo efficacy of the hydrogel in periodontal disease

(1) Clinical observations

The animal study results showed that the model group (Group B) exhibited gingival redness, swelling, tooth mobility, and periodontal pocket formation, indicating successful establishment of the periodontal disease model. In contrast to the model group, the intervention group with the tanshinone IIA nanoparticle-loaded hydrogel (Group E) displayed significantly reduced gingival swelling and bleeding, decreased tooth mobility, and reduced periodontal pocket depth, demonstrating the hydrogel's potent anti-inflammatory and tissue repair capabilities.

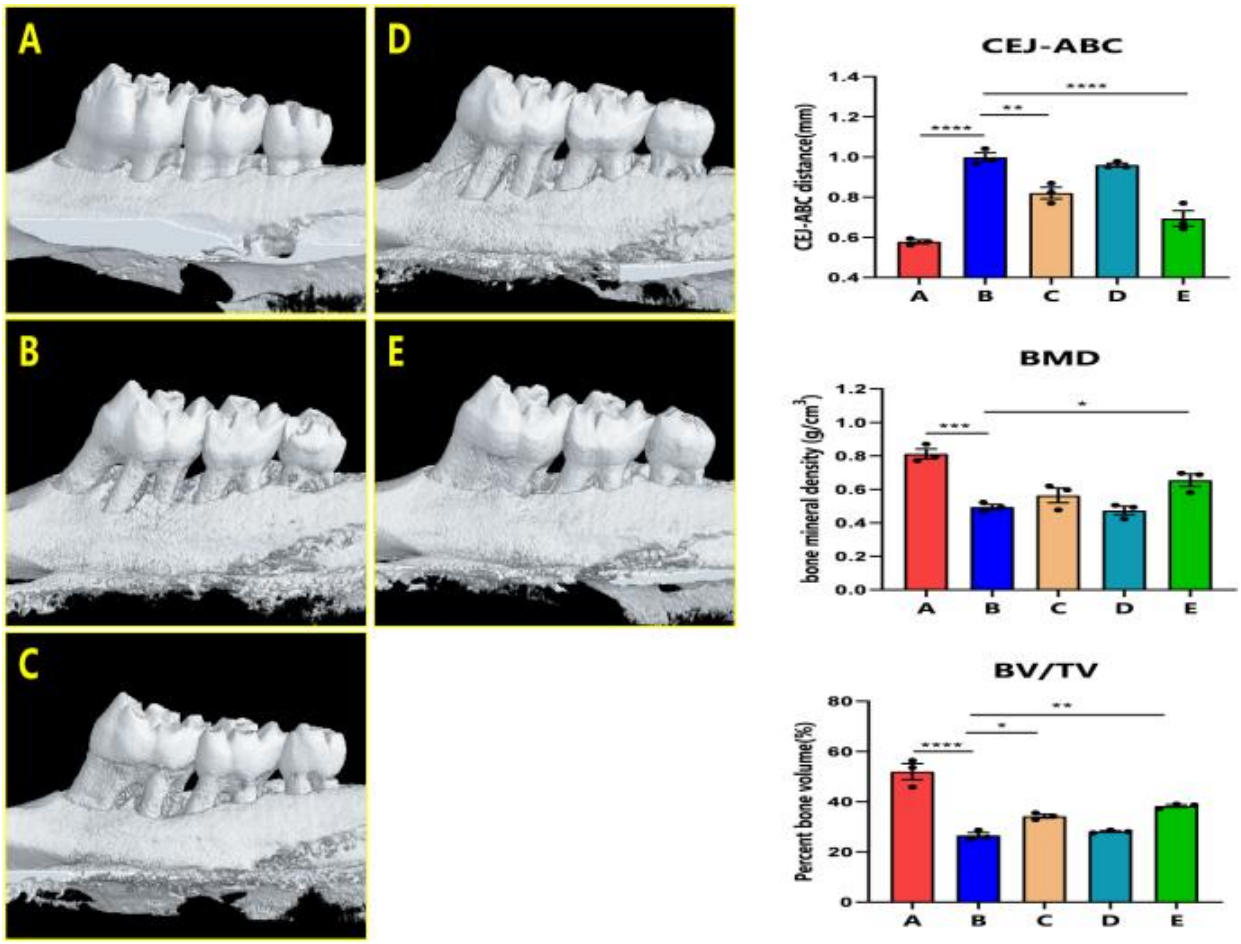

Figure 8. Micro-CT analysis of the left maxillary bone tissue in different groups of rats. **A.** Blank control group. **B.** Model group. **C.** Plain drug intervention group. **D.** Plain hydrogel intervention group. **E.** Drug-loaded hydrogel intervention group. *: $P < 0.05$. **: $P < 0.01$. ***: $P < 0.001$. ****: $P < 0.0001$ *vs*. group B.

(2) Micro-CT analysis

The three-dimensional reconstruction of Micro-CT scans of the left maxillary bone tissue from different groups of rats revealed exposed roots of the first molar, widened periodontal ligament space, and significant alveolar bone loss in groups B and D compared to group A. Groups C and E exhibited less alveolar bone loss than group B with group E showing better results than group C. Micro-CT analysis showed that group B had significantly increased CEJ-ABC and decreased BMD and BV/TV compared to group A. In comparison to group B, groups C and E had significantly decreased CEJ-ABC and increased BV/TV with group E also exhibiting significantly increased BMD (Figure 8).

(3) HE staining

HE staining results displayed that the model group (group B) exhibited significant inflammatory cell infiltration, disrupted periodontal ligament structure, and loosened alveolar bone structure. Compared to the model group, the drug-loaded hydrogel intervention group (group E) had significantly reduced inflammatory cell infiltration, a clear periodontal ligament structure, and a dense alveolar bone structure, indicating that the hydrogel could significantly improve the pathological state of periodontal tissues (Figure 9).

(4) Masson's trichrome staining

Masson's trichrome staining of the maxillary bone tissue from different groups of rats showed

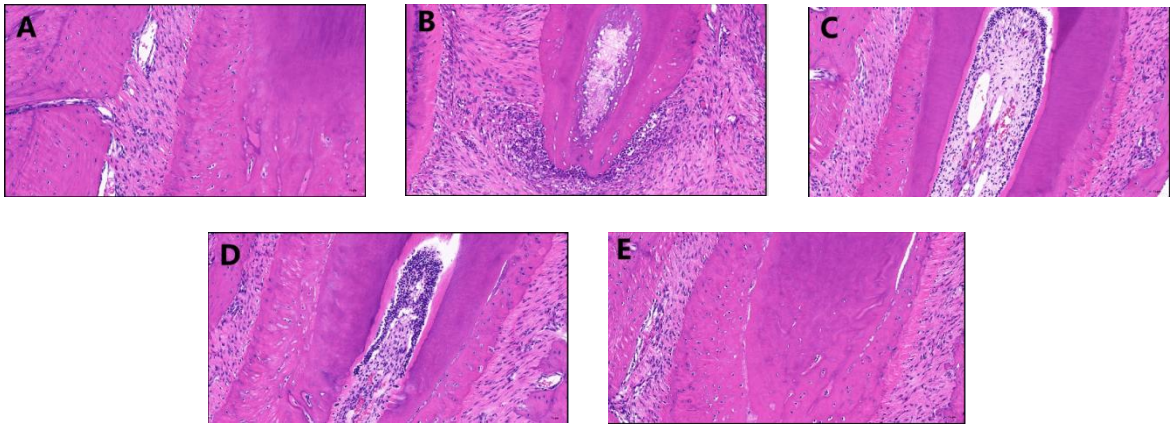

Figure 9. HE staining of the maxillary bone tissue in different groups of rats (200×). **A.** Blank control group. **B.** Model group. **C.** Plain drug intervention group. **D.** Plain hydrogel intervention group. **E.** Drug-loaded hydrogel intervention group.

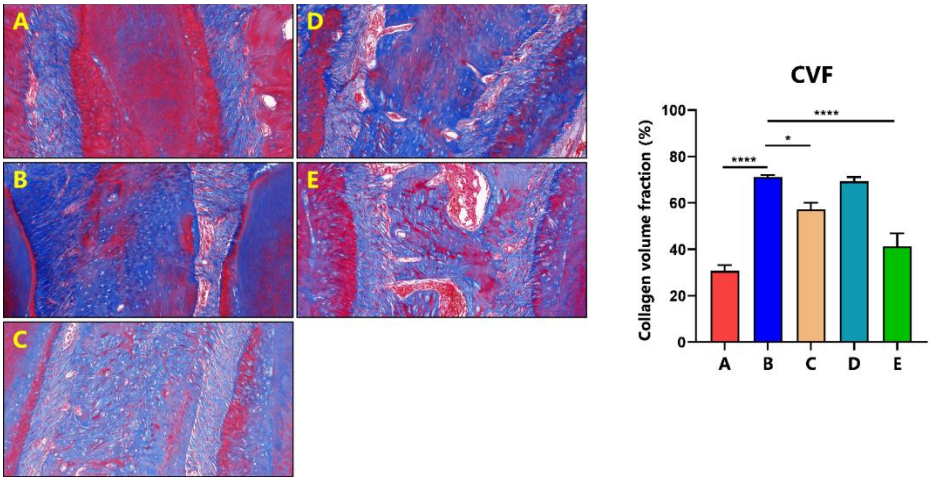

Figure 10. Masson's trichrome staining of the maxillary bone tissue in different groups of rats (200×). **A.** Blank control group. **B.** Model group. **C.** Plain drug intervention group. **D.** Plain hydrogel intervention group. **E.** Drug-loaded hydrogel intervention group. *: $P < 0.05$. **: $P < 0.01$. ***: $P < 0.001$. ****: $P < 0.0001$ *vs*. group B. Collagen fibers stained blue.

that, compared to group A, group B exhibited a significantly increased collagen volume fraction (CVF). In contrast, groups C and E showed a significant decline in CVF compared to group B (Figure 10).

(5) ELISA detection results

The serum levels of IL-1β and IL-18 in different rat groups demonstrated that, compared with group A, the serum concentrations of IL-1β and IL-18 in group B were significantly elevated. When compared to group B, the serum levels of IL-1β and IL-18 in groups C and E were significantly reduced (Figure 11).

Discussion

Periodontitis is a chronic inflammatory disease linked to pathogenic microorganisms and mediated by host immunity, leading to periodontal attachment loss. Chronic periodontitis is most prevalent, making up approximately 95% of all periodontal cases [31]. Currently, mechanical debridement combined with systemic antibiotic therapy is considered an effective treatment for periodontitis [32]. However, the increasing antibiotic resistance amongst periodontal patients may disrupt the normal oral microbiome [33]. Clinical interest in

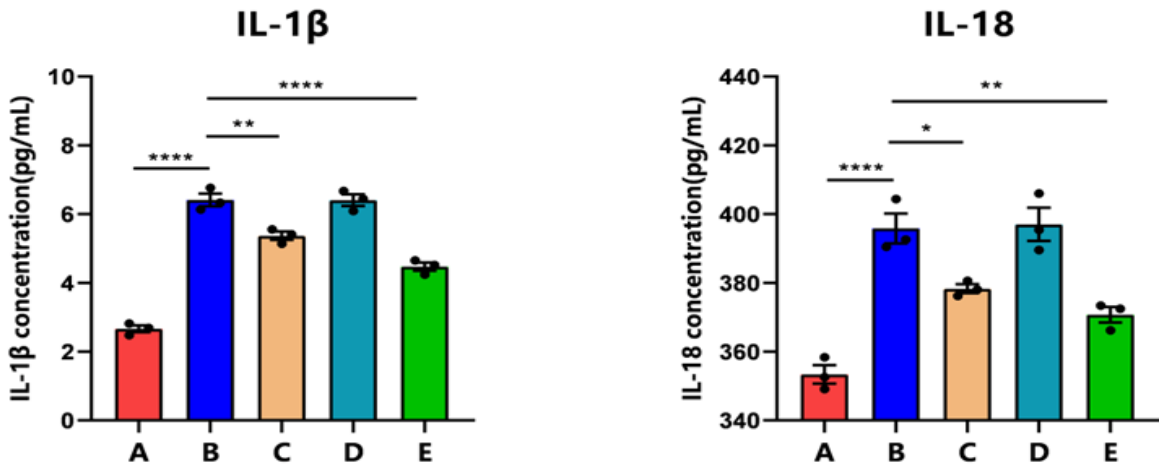

Figure 11. Serum IL-1β and IL-18 Levels in different treatment groups. **A.** Blank control group. **B.** Model group. **C.** Pure drug intervention group. **D.** Pure hydrogel intervention group. **E.** Drug-loaded hydrogel intervention group. *: $P < 0.05$. **: $P < 0.01$. ****: $P < 0.0001$ *vs*. group B.

TCM has grown in recent years because of its multiple effects including anti-inflammatory, hemostatic [34], host immune modulation, and alveolar bone metabolism regulation [35]. Research has shown that certain natural anti-inflammatory agents such as herbal extracts have become a focal point in periodontitis treatment. Asahi *et al*. discovered that catechins significantly reduced ATP levels in periodontal biofilms, thereby inhibiting biofilm metabolism and attenuating the virulence of periodontal pathogens [36]. Furthermore, Zhang *et al*. conducted a study using a Beagle dog periodontitis model and found that the group treated with gallnut sustained-release gel exhibited marked improvements in probing depth (PD), bleeding on probing (BOP), and gingival index (GI). Moreover, the height of newly formed alveolar bone was greater in the gallnut group compared to the PerioChip group, suggesting its potential to promote periodontal tissue regeneration and repair [37]. These findings underscored the potential of natural compounds in periodontal therapy, offering reliable substitutes for conventional antibiotic treatments. *Salvia miltiorrhiza*, a traditional Chinese medicinal herb, has recently garnered attention for its active component, TA, which demonstrates significant effects on bone metabolism regulation and anti-inflammatory processes. Yang *et al*. observed that local oral injection of appropriate doses of Tanshinone IIA effectively promoted alveolar bone remodeling and accelerated orthodontic tooth movement in rabbits [38]. Liu *et al*. reported that Tanshinone IIA at concentrations of 2.5 μM and 5 μM enhanced osteogenic differentiation of human periodontal ligament stem cells (hPDLSCs) [39]. Furthermore, Zhang *et al*. demonstrated that direct injection of Tanshinone IIA into gingival mucosa inhibited osteoclast activity, thereby reducing the relapse distance of the first molar in Wistar rats and increasing the OPG/RANKL ratio [40]. Kim *et al*. found that Tanshinone IIA at 2.5, 5, 10, and 20 μM significantly enhanced the differentiation of C2C12 cells into osteoblasts when continuously administered for 7 days following BMP-2 induction [41]. Moreover, Yao *et al*. reported that supplementing Tanshinone IIA 1 - 2 μg/kg/day for 21 days in an 8-week-old C57BL/6 mouse model induced by PE particles effectively inhibited bone resorption by reducing the number of resorption pits, decreasing the porosity of the cranial bone, and suppressing the activity of TRAP-positive cells [42]. These changes further improved bone volume fraction (BV/TV), bone mineral density, and bone strength. Xin Liu *et al*. further elucidated that Tanshinone IIA induced osteogenesis in hPDLSCs *via* the ERK1/2-Runx2 axis, indicating its potential as a crucial candidate for regenerative periodontal therapy [39].

This research utilized a thermosensitive hydrogel loaded with TA-NPs to improve the delivery and sustained release of TA, aiming to achieve periodontal tissue regeneration. The approach addressed the limitations of traditional delivery methods and enhanced the therapeutic efficacy of Tanshinone IIA in periodontal applications. Based on the previous results and preliminary experimental data, this study set the concentration of nanoparticles at 2 mg/mL, which achieved a good balance between safety and effectiveness. The selection of scaffold materials is crucial in periodontal regenerative therapy. Various scaffold forms have been developed, involving membranes, sponges, fibers, 3D-printed scaffolds, and hydrogels [43]. Among these, hydrogels have garnered significant attention due to their tissue-mimicking capabilities, sustained drug release, and precise site-specific drug delivery [44, 45]. In recent years, thermosensitive hydrogels have made rapid progress. In 2023, Wang *et al*. developed a berberine-loaded thermosensitive hydrogel that rapidly gelated within approximately 3 min at body temperature (37°C). This material demonstrated dual benefits of anti-inflammation and osteogenesis by modulating the PI3K/AKT signaling pathway in periodontal inflammatory bone diseases [46]. Additionally, Yu *et al*. developed a pH-responsive hydrogel containing anti-glycation agents, which showed promise in slowing periodontal disease progression and promoting tissue recovery [47]. Thermosensitive hydrogels, typically liquid or semi-solid at room temperature, can be administered *via* injection and undergo phase transition at the site of application, forming a semi-solid gel [48]. This characteristic has attracted considerable clinical interest [49]. Chitosan (CS), a natural biomaterial, is widely used as a container for medications because of its great biocompatibility and biodegradability [50].

In this study, a novel thermosensitive hydrogel (CS/DEX/β-GP/TA-NPs) loaded with TA-NPs was established, leveraging the advantages of chitosan-based thermosensitive hydrogels. Scanning SEM revealed that the CS/DEX/β-GP hydrogel displayed a uniform three-dimensional porous structure with pore sizes ranging from 100 - 250 μm. Rheological analysis demonstrated significantly enhanced mechanical properties with the addition of DEX. *In vitro* drug release studies displayed sustained release of TA over 7 days with cumulative release rates of approximately 58.0% and 72.9% for CS/DEX/β-GP/TA-NPs and CS/β-GP/TA-NPs, respectively. The hydrogel exhibited excellent biocompatibility, showing no significant cytotoxicity to rat periodontal ligament stem cells (PDLSCs) at various TA-NP concentrations. *In vivo* experiments using a rat periodontitis model showed the anti-inflammatory and bone regenerative effects of the hydrogel. Micro-CT analysis revealed significantly higher bone volume fraction (BV/TV) and bone mineral density (BMD) in the drug-loaded hydrogel intervention group (group E) compared to the model group (group B). Histological analysis using hematoxylin-eosin and Masson's trichrome staining showed reduced inflammatory cell infiltration and enhanced periodontal ligament structure in group E, indicating the ability of hydrogel to improve periodontal tissue pathology and promote normal repair. ELISA results further confirmed the anti-inflammatory effect of the hydrogel with significantly lower levels of IL-1β and IL-18 in group E compared to group B.

This study successfully developed a TA-NP-loaded thermosensitive hydrogel that demonstrated excellent biocompatibility and therapeutic efficacy in both *in vitro* and *in vivo* experiments. The research provided a novel approach and experimental basis for applying TCM in periodontal disease treatment and offered promising potential for developing innovative periodontal tissue regeneration materials. Future research should focus on optimizing hydrogel formulations and conducting clinical trials to further validate its therapeutic efficacy and safety in humans.

References

1. Sedghi LM, Bacino M, Kapila YL. 2011. Periodontal disease: The good, the bad, and the unknown. Front Cell Infect Microbiol. 11:766944.
2. Hajishengallis G, Chavakis T, Lambris JD. 2000. Current understanding of periodontal disease pathogenesis and targets for host-modulation therapy. Periodontol 2000. 84:14-34.
3. Laberge S, Akoum D, Wlodarczyk P, Massé J-D, Fournier D, Semlali A. 2023. The potential role of epigenetic modifications on different facets in the periodontal pathogenesis. Genes. 14:1202.
4. Eke PI, Wei L, Borgnakke WS, Thornton-Evans G, Zhang X, Lu H, *et al*. 2016. Periodontitis prevalence in adults ≥ 65 years of age in the USA. Periodontol 2000. 72:76-95.
5. Hajishengallis G. 2022. Interconnection of periodontal disease and comorbidities: Evidence, mechanisms, and implications. Periodontol 2000. 89:9-18.
6. Kapila YL. 2021. Oral health's inextricable connection to systemic health: Special populations bring to bear multimodal relationships and factors connecting periodontal disease to systemic diseases and conditions. Periodontol 2000. 87:11-16.
7. Nibali L, Gkranias N, Mainas G, Di Pino A. 2022. Periodontitis and implant complications in diabetes. Periodontol 2000. 90:88-105.
8. Parsegian K, Randall D, Curtis M, Ioannidou E. 2022. Association between periodontitis and chronic kidney disease. Periodontol 2000. 89:114-124.
9. Herrera D, Sanz M, Shapira L, Brotons C, Chapple I, Frese T, *et al*. 2023. Association between periodontal diseases and cardiovascular diseases, diabetes and respiratory diseases: Consensus report of the Joint Workshop by the European Federation of Periodontology (EFP) and the European arm of the World Organization of Family Doctors (WONCA Europe). J Clin Periodontol. 50:819-841.
10. Xu B, Han YW. 2022. Oral bacteria, oral health, and adverse pregnancy outcomes. Periodontol 2000. 89:181-189.
11. Koziel J, Potempa J. 2022. Pros and cons of causative association between periodontitis and rheumatoid arthritis. Periodontol 2000. 89:83-98.
12. Radaic A, Ganther S, Kamarajan P, Grandis J, Yom SS, Kapila YL. 2021. Paradigm shift in the pathogenesis and treatment of oral cancer and other cancers focused on the oralome and antimicrobial-based therapeutics. Periodontol 2000. 87:76-93.
13. Haque MM, Yerex K, Kelekis-Cholakis A, Duan K. 2022. Advances in novel therapeutic approaches for periodontal diseases. BMC Oral Health. 22:492.
14. Forouzanfar F, Forouzanfar A, Sathyapalan T, Orafai HM, Sahebkar A. 2020. Curcumin for the management of periodontal diseases: A review. Curr Pharm Des. 26:4277-4284.
15. Rams TE, Degener JE, Van Winkelhoff AJ. 2014. Antibiotic resistance in human chronic periodontitis microbiota. J Periodontol. 85:160-169.
16. Zu R, Yi H, Yi Y, Yong J, Li Y. 2019. Effect of cryptotanshinone on *Staphylococcus* epidermidis biofilm formation under *in vitro* conditions. Jundishapur J Microbiol. 12:e83922.
17. Zhou S, Chen W, Su H, Zheng X. 2013. Protective properties of tanshinone I against oxidative DNA damage and cytotoxicity. Food Chem Toxicol. 62:407-412.
18. Kim HH, Kim JH, Kwak HB, Huang H, Han SH, Ha H, *et al*. 2004. Inhibition of osteoclast differentiation and bone resorption by tanshinone IIA isolated from *Salvia miltiorrhiza* Bunge. Biochem Pharmacol. 67:1647-1656.
19. Cai Y, Zhang W, Chen Z, Shi Z, He C, Chen M. 2016. Recent insights into the biological activities and drug delivery systems of tanshinones. Int J Nanomed. 11:121-130.
20. Shan X, Bangzhen H, Liu J, Wang G, Chen W, Yu N, *et al*. 2021. Review of chemical composition, pharmacological effects, and clinical application of *Salviae Miltiorrhizae* Radix et Rhizoma and prediction of its Q-markers. China J Chin Mater Med. 46:5496-5511.
21. Ashour AA, Ramadan AA, Abdelmonsif DA, El-Kamel AH. 2020. Enhanced oral bioavailability of Tanshinone IIA using lipid nanocapsules: Formulation, *in vitro* appraisal and pharmacokinetics. Int J Pharm. 586:119598.
22. Xu Y, Luo C, Wang J, Chen L, Chen J, Chen T, *et al*. 2021. Application of nanotechnology in the diagnosis and treatment of bladder cancer. J Nanobiotechnol. 19:1-18.
23. Shaikh J, Ankola D, Beniwal V, Singh D, Kumar MR. 2009. Nanoparticle encapsulation improves oral bioavailability of curcumin by at least 9-fold when compared to curcumin administered with piperine as absorption enhancer. Eur J Pharm Sci. 37:223-230.
24. Swarnakar NK, Jain AK, Singh RP, Godugu C, Das M, Jain S. 2011. Oral bioavailability, therapeutic efficacy and reactive oxygen species scavenging properties of coenzyme Q10-loaded polymeric nanoparticles. Biomaterials. 32:6860-6874.
25. Zhang W. Construction of biomimetic hydrogel scaffolds with slow drug release for facilitating cartilage repair. Southern Medical University, 2021.
26. Kim IY, Seo SJ, Moon HS, Yoo MK, Park IY, Kim BC, *et al*. 2008. Chitosan and its derivatives for tissue engineering applications. Biotechnol Adv. 26:1-21.
27. Jia H, Wang X, Li X, Liu Y. 2010. Experimental study on synergistic antiplaque effect of chitosan and chlorhexidine. Chin J Geriatr Dent. 8:24-26.
28. Bhattarai N, Gunn J, Zhang M. 2010. Chitosan-based hydrogels for controlled, localized drug delivery. Advanced drug delivery reviews. 62:83-99.
29. Chen P, Liu L, Pan J, Mei J, Li C, Zheng Y. 2019. Biomimetic composite scaffold of hydroxyapatite/gelatin-chitosan core-shell nanofibers for bone tissue engineering. Mater Sci Eng C. 97:325-335.
30. Wu J, Wei W, Wang LY, Su ZG, Ma GH. 2007. A thermosensitive hydrogel based on quaternized chitosan and poly (ethylene glycol) for nasal drug delivery system. Biomaterials. 28:2220-2232.
31. Ustianowska K, Ustianowski Ł, Bakinowska E, Kiełbowski K, Szostak J, Murawka M, *et al*. 2024. The genetic aspects of periodontitis pathogenesis and the regenerative properties of stem cells. Cells. 13:117.
32. Kepic TJ, O'Leary TJ, Kafrawy AH. 1990. Total calculus removal: An attainable objective? J Periodontol. 61:16-20.
33. Matthews DC. 2014. Prevention and treatment of periodontal diseases in primary care. Evid Based Dent. 15:68-69.

34. Moghadam ET, Yazdanian M, Tahmasebi E, Tebyanian H, Ranjbar R, Yazdanian A, *et al*. 2020. Current herbal medicine as an alternative treatment in dentistry: *In vitro*, *in vivo* and clinical studies. Eur J Pharmacol. 889:173665.
35. Shi J, Yang Y, Qin R, Shi C, Dong X. 2022. Research progress on traditional Chinese medicine in the treatment of periodontal disease. J China Prescr Drug. 20:171-174.
36. Asahi Y, Noiri Y, Miura J, Maezono H, Yamaguchi M, Yamamoto R, *et al*. 2014. Effects of the tea catechin epigallocatechin gallate on Porphyromonas gingivalis biofilms. J Appl Microbiol. 116:1164-1171.
37. Zhang S. Experimental study on the promotion of periodontal tissue regeneration by Wu Bei Zi sustained-release gel. Fourth Military Medical University, 2010.
38. Yang X, Zhang J, Wang X, Hong A, Mo C. 2015. Effect of local injections of tanshinone II-A on VEGF expression of periodontal membrane in rabbit orthodontic tooth movement. J Guiyang Med Coll. 40:467-470.
39. Liu X, Niu Y, Xie W, Wei D, Du Q. 2019. Tanshinone IIA promotes osteogenic differentiation of human periodontal ligament stem cells via ERK1/2-dependent Runx2 induction. Am J Transl Res. 11:340.
40. Zhang S, Liu J, Zhao G. 2014. Expression of osteoclast differentiation factors during relapse stage after local injection of Danshensu IIA in orthodontic tooth movement. Chin J Tissue Eng Res. 18:1730-1736.
41. Kim HJ, Kim SH. 2010. Tanshinone IIA enhances BMP-2-stimulated commitment of C2C12 cells into osteoblasts *via* p38 activation. Amino Acids. 39:1217-1226.
42. Yao J, Ma S, Feng W, Wei Y, Lu H, Zhong G, *et al*. 2018. Tanshinone IIA protects against polyethylene particle-induced osteolysis response in a mouse calvarial model. Int J Clin Exp Pathol. 11:4461.
43. Santos MS, Dos Santos AB, Carvalho MS. 2023. New insights in hydrogels for periodontal regeneration. J Funct Biomater. 14:545.
44. Zhang W, Du A, Liu S, Lv M, Chen S. 2021. Research progress in decellularized extracellular matrix-derived hydrogels. Regener Ther. 18:88-96.
45. Ayala-Ham A, López-Gutierrez J, Bermúdez M, Aguilar-Medina M, Sarmiento-Sánchez JI, López-Camarillo C, *et al*. 2021. Hydrogel-based scaffolds in oral tissue engineering. Front Mater. 8:708945.
46. Wang S, Shao C, Zhao X, Guo Y, Song H, Shen L, *et al*. 2024. Application of three-dimension printing nano-carbonated-hydroxylapatite to the repair of defects in rabbit bone. Int J Nanomed. 19:1667-1681.
47. Yu F, Geng D, Kuang Z, Huang S, Cheng Y, Chen Y, *et al*. 2022. Sequentially releasing self-healing hydrogel fabricated with TGFβ3-microspheres and bFGF to facilitate rat alveolar bone defect repair. Asian J Pharm Sci. 17:425-434.
48. Liu Y, Ding L, Chen G, Wang P, Wang X. 2024. A thermo-sensitive hydrogel with prominent hemostatic effect prevents tumor recurrence *via* anti-anoikis-resistance. J Nanobiotechnol. 22:496.
49. Thambi T, Li Y, Lee DS. 2017. Injectable hydrogels for sustained release of therapeutic agents. J Control Release. 267:57-66.
50. Li M, Lv J, Yang Y, Cheng G, Guo S, Liu C, *et al*. 2022. Advances of hydrogel therapy in periodontal regeneration - a materials perspective review. Gels. 8:624.